

Bismuth based Half Heusler Alloys with giant thermoelectric figure of merit

Vikram,[†] Jiban Kangsabanik,[†] Enamullah[†] and Aftab Alam^{*}

Department of Physics, Indian Institute of Technology, Bombay, Powai, Mumbai 400 076, India

Half Heusler (HH) thermoelectric alloys provide a wide platform to choose materials with non-toxic and earth abundant elements. This article presents an *ab-initio* theoretical evaluation of electrical and thermal transport properties of three Bismuth-based most promising thermoelectric alloys, selected out of 54 stable HH compounds. These are brand new compounds which are recently proposed to be stable (Nature Chem. **7**, 308 (2015)) and may have interesting properties. The calculated band structure of the three compounds, namely HfRhBi, ZrIrBi and ZrRhBi, served as a hint for their promising thermoelectric properties. To gain confidence on the theoretical predictions of these unreported systems, we first checked our calculated results for a well studied similar compound, ZrNiSn, and showed reasonable agreement with the measured ones. HfRhBi and ZrIrBi turn out to be narrow band gap while ZrRhBi is a moderate band gap semiconductor. A detailed study of the carrier concentration and temperature dependance of the Seebeck coefficient (S), Power factor ($S^2\sigma$), lattice (κ_L) and electronic (κ_e) thermal conductivity and hence the figure of merit (ZT) is carried out. In contrast to most promising known thermoelectric materials, we found high power factor for these materials (highest $S^2\sigma \sim 17.36 \text{ mWm}^{-1}\text{K}^{-2}$ for p-type ZrIrBi). All the three systems (specially p-type) show high figure of merit, with ZT value as high as 0.45 for ideal crystal. Maximum ZT and the corresponding optimal n- and p-type doping concentrations (n_c) are calculated for all the three compounds, which shall certainly pave guidance to future experimental work.

PACS numbers: 31.15.A-, 72.20.Pa, 84.60.Rb, 63.20.kd, 61.72.-y

INTRODUCTION

The ever increasing demand of energy rests on a concerted effort to broaden our energy resources (solar, fuel, wind, etc.) and at the same time reduce our energy consumption. As a matter of fact, a large fraction of energy consumed throughout the globe is lost as heat, and conversion of even a small fraction of it to other form of usable energy can significantly impact the globe energy requirement. Significant efforts are underway to convert these waste heat into electricity using thermoelectrics. In addition, advances in thermoelectrics lead to the development of multistage Peltier coolers which can be used to achieve efficient cooling/heating.

The fundamental requirement to obtain a promising thermoelectric material is to optimize a variety of conflicting properties. The conversion efficiency of thermoelectric (TE) materials depends upon the transport coefficients of the constituent material through a dimensionless figure of merit, $ZT = (S^2\sigma T) / (\kappa_e + \kappa_L)$. Here, S , σ and T are the Seebeck coefficient, electrical conductivity and temperature respectively. κ_e (κ_L) are the thermal conductivity due to electrons (phonons).

The value of ZT measures how efficient the material is for both TE heating/cooling applications, higher the value higher the efficiency. The main challenge among the researchers is how to enhance the value of ZT since the transport parameters S , σ and κ (κ_e and κ_L) are

inter-related to each other. The electronic thermal conductivity and electrical conductivity is related to each other by the Wiedemann-Franz law, $\kappa_e = L\sigma T$, where L is the Lorentz number. This relation clearly shows that increasing electrical conductivity also increases electronic thermal conductivity hence optimization of ZT turns out to be challenging. In earlier days, metals were used for TE applications because of very good electrical conductivity but their ZT values were low since metals possess large thermal conductivity with significant contribution from the lattice part (κ_L). Hence minimizing lattice thermal conductivity is itself a challenge. Most popular TE materials are based upon Bi_2Te_3 and $\text{Si}_{1-x}\text{Ge}_x$ having ZT value above 1 at their optimal temperature.[2]·[3] Other bulk materials, such as complex chalcogenides,[4]·[5] skutterudites[6]·[7] and quasicrystals[8] are potential candidates for TE applications.

Heusler alloys have been known to mankind since the beginning of the 20th century. They are known to have a very rich magnetic behaviour which make them a promising candidate for spintronic applications.[9] Good electrical and mechanical properties, thermal stability and easy tunability of band gap (0-4 eV) by only changing the chemical composition makes them potential candidates for solar cell applications and topological insulators[9]. But in the last decade, ternary half-Heusler alloys (HHAs) have emerged as promising candidates for TE applications also due to small value of band gap, high value of Seebeck coefficient (S) (upto several hundreds μVK^{-1}) and its appealing transport properties.

A very big advantage of considering HHAs for thermo-

[†] These three authors have contributed equally to this work

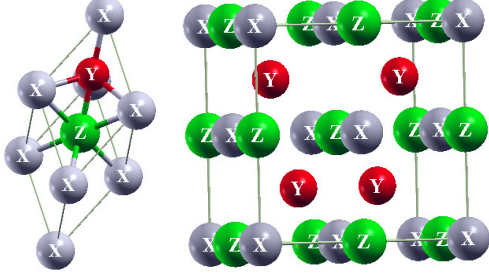


FIG. 1. A 3-atom primitive cell (left) and a cubic unit cell (right) of HHAs XYZ, where X represents either Hf or Zr, Y as either Rh or Ir; and Z as Bi.

electric application is that they can be easily synthesized as 100% dense samples[10] and the efficiency (i.e. ZT) can be enhanced by the application of easy doping (either with n-type or p-type) or by inducing impurities or defects. Another reason to consider HHAs is the high value of their power factor ($S^2\sigma$) which is one of the most important criteria for TE applications.

HHAs can serve as high as well as moderate temperature TE materials and have the potential to replace some of the state of art TE materials.[11]–[21] In the last few years, there has been extensive efforts to find new HHAs as potential TE materials. Until now, the most reliable HH compound found are the family of $MNiSn$ ($M=Ti, Zr, Hf$) - related compounds with the maximum ZT values lying in range 0.7-1.5.[22]–[24] However, this $(ZT)_{max}$ is achieved by playing with various types of doping (e.g. mixing M-elements with each other or doping Sb with Sn etc.), nanostructuring etc. The maximum ZT obtained for ideal crystal of $ZrNiSn$ (no doping), however, remains 0.2 – 0.3.[22] Among others, $NbCoSn$ ($ZT \sim 0.15$),[25] $TiCoSb$ ($ZT \sim 0.015$),[26] etc. emerge out to be good TE HH compounds. The main reason for not getting high value of ZT in ideal crystals of HHAs is the high values of thermal conductivity and relatively lower values of power factor. For example, the experimentally determined maximum power factor for $ZrNiSn$ -based alloy [22] is $3.4 \text{ mWm}^{-1}\text{K}^{-2}$ at 750 K, and for $TiCoSb$ -based alloy[27] is $2.3 \text{ mWm}^{-1}\text{K}^{-2}$ at 850 K. Although, these power factors are relatively higher than those of most current TE materials, but not as high as to enhance the figure of merit to a great extent. On the other hand, ultra low thermal conductivity has been found recently in $YNiBi$ system, [28] but with a very low ZT.

Although, there exists several ideal HH crystals with relatively high ZT values, however the hunt for more such alloys is still ongoing in order to find better TE materials. In fact, if one look at the Inorganic Crystal Structural Database (ICSD) [29] or Pearsons hand book [30] there exists hundreds of HH alloys. More recently, a huge database[1] is created for such alloys with

the total valance electron count (VEC) in their primitive unit cell to be 18. Their main motivation was to report chemically plausible compounds that can have interesting properties but were neglected in the past. They mainly checked the stability and some basic electronic structure properties of these compounds using high throughput first principle calculations. Because HH compounds with $VEC=18$ have narrow band gaps and show promising TE properties, we have done a detailed band structure calculation[31] of all the stable compounds reported in Ref. [1]. Topology of these band structures helped to identify three compounds $HfRhBi$, $ZrIrBi$ and $ZrRhBi$ which turn out to be quite promising with the maximum ZT reaching upto ~ 0.45 .

The purpose of this paper is to systematically evaluate and present a detailed electronic structure, electrical as well as thermal transport properties of these three alloys. The key features of the present study which make it superior (with a higher predictability) compared to other theoretical studies existing in the literature are as follows,

1. Most current theoretical work on the topic of thermoelectricity are simply based on the density of states, formation of energy gaps, [32]–[33]–[34] related chemical interaction between the d-states of transition metal,[32]–[33] compositional dependence of electronic structure, etc. In more recent articles people have looked at some aspects of electrical transport as well.[35]–[36] The thermal transport arising from the phonons, however, is mostly ignored. In this paper we have considered both electrical and thermal transport on the same footing so as to report the most reliable values of ZT.
2. In most previous studies, Seebeck coefficient (S) or electrical conductivity (σ) or the power factor ($S^2\sigma$) [35] or at best $S^2\sigma/\kappa_e$ is chosen as the parameter to dictate the thermoelectric performance or the optimal n-type or p-type doping levels for the concerned compound. However the ideal parameter should have been ZT as at low and moderate temperatures the lattice thermal conductivity (κ_L) plays an important role. Here, we have chosen ZT to be the comprehensive parameter to do the same and all the thermoelectric parameters reported in this paper corresponds to that optimal $(ZT)_{max}$.
3. A detailed phonon based analysis (phonon dispersion, phonon density of states), usually ignored in most literature, is performed here (see supplement [54]) to better understand the effect of lattice dynamics.
4. Mechanical stability for these class of compounds has been seldom reported.[37]–[40] Keeping the device fabrication and application in mind, we have calculated the elastic constants, Bulk modulus (B)

system	$a(\text{\AA})$	$\Delta E_g(\text{eV})$	$\Delta E_f(\text{eV/atom})$
HfRhBi	6.41	0.17	-0.651
ZrIrBi	6.48	0.26	-0.315
ZrRhBi	6.44	1.02	-0.725

TABLE I. Band gap (ΔE_g) and formation energy (ΔE_f) at theoretically relaxed lattice constant (a).

and the Young's modulus (Y) to assert the robustness of these systems against various stress.

COMPUTATIONAL AND THEORETICAL DETAILS

Ab-initio simulations are performed by using density functional theory (DFT)[41] implemented within Vienna *ab-initio* simulation package (VASP)[42]–[44] with a projected augmented-wave basis.[45] We used the Generalized Gradient Approximation (GGA) with Perdew-Burke-Ernzerhof (PBE)[46] scheme for the electronic exchange-correlation functional. A plane wave cut-off of 500 eV was used in all the calculations. Tetrahedron method with Blöchl corrections [47] were used to calculate the Density of states (DOS). Electronic structure optimization was converged within the energy error $\sim 10^{-5}$ eV. Cell volume, shape and atomic positions for all the structures were fully relaxed using conjugate gradient algorithm till the forces on each atom falls below 0.01 eV/Å. The Brillouin zone sampling was done by using Automated Γ -centered K point mesh. A $20 \times 20 \times 20$ K point mesh was used to do the ionic relaxation as well as the self consistent calculations.

The thermoelectric properties of suitable candidates were then calculated using the BoltzWann module[48] of Wannier90 package.[49] This uses Maximally Localised Wannier Function (MLWF) basis set[50]–[51] by interpolating first principle plane wave results to determine the Seebeck coefficient (S), electrical conductivity (σ) and the electronic part of the thermal conductivity (κ_e) using semi classical Boltzmann transport theory. The calculations were performed within a constant relaxation time approximation scheme ($\tau=10$ fs). For transport calculations, we took 24 bands and 20 wannier functions for all the three systems. The frozen window was taken around the Fermi level (E_F) in such a way that it included all the states withing 2 eV range above and below the conduction and valence band edges respectively.

The properties for n-type and p-type materials were evaluated based on rigid band approximation. According to it the addition of donor or acceptor atom does not affect the band structure of the material, but instead causes the chemical potential to shift. The chemical potential moves towards the conduction bands as electron doping increase and goes towards the valence bands as

system	C_{11}	C_{12}	C_{44}	B	Y
HfRhBi	198.29	92.29	47.95	127.62	133.79
ZrIrBi	211.60	94.19	55.28	133.33	149.64
ZrRhBi	194.14	86.96	50.13	122.69	136.37

TABLE II. Calculated elastic constants C_{ij} , Bulk modulus (B) and Young's modulus (Y) (all in GPa) at theoretically relaxed lattice constant.

the hole doping increases. The output of the BoltzWann package is in terms of properties varying with respect to the chemical potential (μ). In order to study the transport properties in terms of the carrier concentration (n_c) instead of the chemical potential, we use the equation $n_c = \int D(E)f(E)dE$, where $D(E)$ is the density of states and $f(E)$ is the Fermi-Dirac distribution function for electrons of energy E . At a fixed temperature, the integral can be performed over entire energy range at a given chemical potential to give the corresponding carrier concentration value or vice versa.

To calculate the lattice contribution to the thermal conductivity (κ_L) we use Boltzmann transport theory for phonons as implemented in ShengBTE package.[52] For this, we calculated the 2nd order inter-atomic force constants (IFCs) using PHONOPY package[53]. The 3rd order IFCs are calculated using thirdorder.py module of ShengBTE package using small displacement method which generate atomic configuration files with required displacements. Here we took $4 \times 4 \times 4$ super-cell to accurately calculate the force constants for both 2nd order and 3rd order IFC calculations. Interactions up to fourth nearest neighbour is taken into account for the calculation of 3rd order force constants. The Born effective charges on each atom and the macroscopic dielectric tensor is calculated using Density functional perturbation theory on the primitive cell using $16 \times 16 \times 16$ k-mesh.

HHAs have a general composition of XYZ, where X and Y are low and high electronegative transition elements and Z is a main group element. HHA crystallizes in MgAgAs type structure (space group F-43m (#216)), as shown in Figure 1. Our structural optimization suggest that the most stable structure is the one with X at 4a(0,0,0), Y at 4c(0.25, 0.25, 0.25) and Z at 4b(0.5, 0.5, 0.5) wyckoff positions. For the TE analysis, specially to calculate the lattice thermal conductivity of the system, we made a super cell of $4 \times 4 \times 4$ from a 3-atom primitive cell (shown in Figure 1).

Further computational details about the formation energies and the mechanical properties are given in the supplementary material.[54]

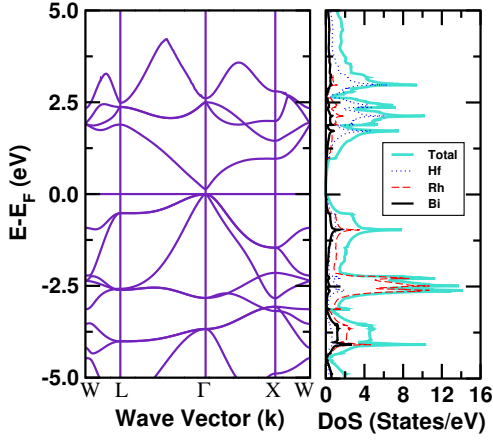


FIG. 2. Band structure(left) and atom projected DOS(right) of HfRhBi.

RESULTS AND DISCUSSION

The detailed theoretical analysis of chemical stability, electronic structure, mechanical stability and TE properties for the three systems HfRhBi, ZrIrBi and ZrRhBi are summarized in this section. Table I presents the theoretically relaxed lattice parameters, the formation energies and the direct band gap values obtained from the electronic structure calculations. Large negative values of formation energies make these systems quite stable to external changes. The low band gap (≤ 1 eV) make them potential candidates as TE material.

As discussed, since the mechanical stability of the material is an important property for it to be used for device fabrication, and hence for thermoelectric application, we also calculated the elastic constants for the three systems. The relevant parameters required to check the mechanical stability of the material as per the Born-Huang criteria (see supplement[54] for details) are listed in Table II. These parameters satisfy all the criteria required for mechanical stability of all the three systems. The calculated values of elastic constants (B and Y) are comparable to those for standard metals. This suggests that they can be cut or drawn into different shapes without changing the properties up to a fairly high point.

HfRhBi

Electronic Structure : Figure 2 shows the band structure and atom projected DOS for HfRhBi. It has a direct band gap of 0.173 eV at Γ point. This low value of the band gap aids easy excitation of thermally excited electrons increasing the electrical conductivity. Flat bands (causing a sharp DOS) at/near the valence band maxima near E_F suggest a high value of effective mass for holes implying that this material can be used as a potentially good p-type TE material. Since the conduction

band states are very sharp near E_F , the n-type figure of merit is expected to be lesser than the p-type. High bulk modulus (≈ 127.6 GPa), Young's modulus (≈ 133.8 GPa) (see Table II) along with the strong chemical stability suggests the material to remain robust in structure and electronic properties against pressure or other stress.

Thermoelectric properties: Figure 3 shows the Seebeck coefficient (S), Power factor ($S^2\sigma$), thermal conductivity κ (both lattice and electronic) and the figure of merit (ZT) as a function of carrier concentration n_c (left) and temperature (T) (right) for both n-type and p-type HfRhBi. The n_c dependence of all the quantities are shown at six different temperatures (T). Two optimal doping concentrations [one each for $(ZT)_{max}$ at 1300 K and 900 K] are then chosen to plot the temperature dependence (right panel) for the same quantities.

As evident from the figure, the Seebeck coefficient for p-type first increases with n_c , reaching a maximum and then decreases with further increase in n_c . The behavior for n-type, however, is completely different. In the concentration range $\sim 10^{20}$ - 10^{22} cm $^{-3}$, the electrical conductivity (σ) increases rapidly, and dominate the behavior of the power factor vs. n_c . This corresponds to an optimal carrier concentration, $(n_c)_{max}$, based on the maxima in the power factor ($S^2\sigma$) at a given temperature. However, looking at the variation of thermal conductivity (κ) vs. n_c , κ shows a maximum at a relatively higher concentration than the optimal concentration, as estimated using $S^2\sigma$. This changes the value of the optimal carrier concentration at which ZT achieves the maximum value. As such, the most common practice [35] for estimating the optimal concentration based on a maxima in the $S^2\sigma$ is misleading. The variation of the thermal conductivity and hence its effect on ZT, can completely change the value of $(n_c)_{max}$. We have chosen the n_c dependence of ZT (instead of $S^2\sigma$) to obtain the optimal carrier concentrations, $(n_c)_{max}$. The temperature dependence is plotted for one more carrier concentration having ZT value $\sim 80\%$ of the $(ZT)_{max}$ for comparison sake (1.96×10^{20} cm $^{-3}$ for n-type and 1.03×10^{20} cm $^{-3}$ for p-type).

For p-type HfRhBi, the maximum power factor came out to be ≈ 10.88 mWm $^{-1}$ K $^{-2}$ at 1300 K. At such a high temperature, due to thermally excited electron-hole pairs, the electronic part of thermal conductivity (κ_e) becomes very large but at the same time lattice thermal conductivity (κ_L) decreases drastically due to decrease in the mean free path (L_{ph}) of the highly agitated phonons. The ZT value comes out to be 0.37. Even at smaller temperatures (800-1000 K), power factor lies in the range ≈ 6.2 - 8.4 mWm $^{-1}$ K $^{-2}$ which is much larger than the values obtained for most promising HH thermoelectric materials e.g. ≈ 3.4 mWm $^{-1}$ K $^{-2}$ for ZrNiSn, [22] ≈ 2.3 mWm $^{-1}$ K $^{-2}$ for TiCoSb.[27]

For n-type HfRhBi at 1300 K, the Seebeck coefficient is less than that of p-type. This is due to a lower value of the effective mass in the n-region, as obvious from the

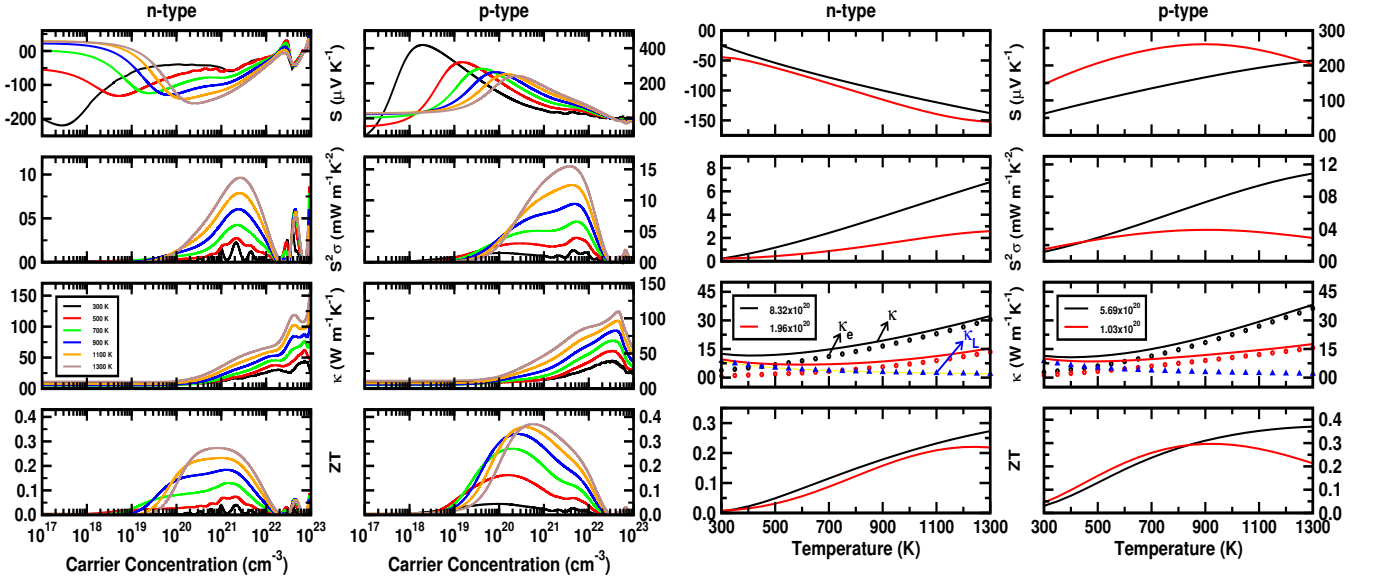


FIG. 3. (Left) Carrier concentration dependence of Seebeck coefficients (S), power factor ($S^2\sigma$), thermal conductivity [lattice (κ_L), electronic (κ_e) and total (κ)] and figure of merit (ZT) for n and p-type HfRhBi alloy at various temperatures (T). (Right) Temperature dependence of the same quantities for n and p-type HfRhBi at two different optimal concentrations.

band structure. The power factor and hence the ZT is also smaller. The optimal value of ZT at 1300 K is 0.27.

ZrIrBi

Electronic Structure : Band structure and atom projected density of states for ZrIrBi are shown in Fig. 4. This system has similar band structure as HfRhBi near E_F except for the fact that the top most valence band is more flat and the conduction band edges are more steeper near Γ point. Thus one can expect the Seebeck coefficient and power factor for ZrIrBi to be relatively higher than that of HfRhBi for p-type system. Whereas the steeper

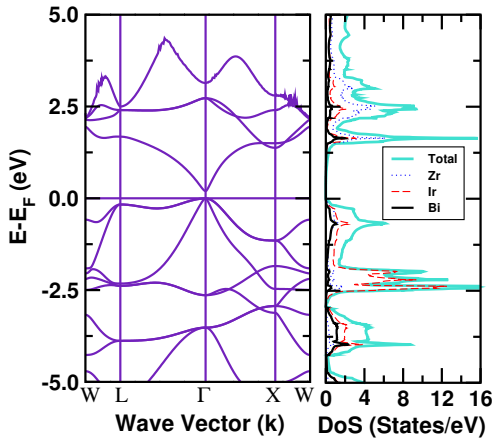


FIG. 4. Band structure(left) and atom projected DOS(right) of ZrIrBi.

conduction bands and a very slow rise in the value of DOS above E_F suggest it to have lower S and hence ZT value than HfRhBi for n-type system. ZrIrBi has highest mechanical stability out of the three systems with the bulk modulus ≈ 133.3 GPa and Young's modulus ≈ 149.6 GPa (Table II).

Thermoelectric properties: The variation of relevant quantities (S , $S^2\sigma$, κ and ZT) with carrier concentration (left) and temperature (right) are shown in Fig. 5. Similar to HfRhBi, ZrIrBi is a good p-type TE material. Compared to HfRhBi, it has a large power factor and low lattice thermal conductivity (≈ 2 Wm $^{-1}$ K $^{-1}$) at intermediate as well as higher temperature range. At optimal carrier concentration (n_c) $_{max} = 8.79 \times 10^{20}$ cm $^{-3}$, it has a Seebeck Coefficient of $255.9 \mu\text{VK}^{-1}$ and electrical conductivity of $26.5 \times 10^4 \Omega^{-1}\text{m}^{-1}$ yielding the power factor to be as large as $\approx 17.4 \text{ mWm}^{-1}\text{K}^{-2}$ (at $T=1300$ K). This gives a ZT value of 0.42. Notably, the ZT -value does not reduce much until 900 K ($ZT \approx 0.38$). As such, p-type ZrIrBi can be used as a promising TE material even at relatively low T .

For n-type system, one can notice a shallower increase in the DOS near conduction band edge arising out of steep bands near E_F (see Fig. 4), thus making the effective mass relatively small and hence giving smaller value of Seebeck coefficient ($95.6 \mu\text{VK}^{-1}$ at 1300 K). Since at high temperature, the contribution of κ_L to total thermal conductivity is very small, so ZT effectively depends on the S value ($ZT \approx S^2/L$, where L is the Lorentz number). Thus in spite of having a high σ value ($79.7 \times 10^4 \Omega^{-1}\text{m}^{-1}$, which is almost double to that of HfRhBi), ZT (0.21) for ZrIrBi turn out to be smaller than HfRhBi.

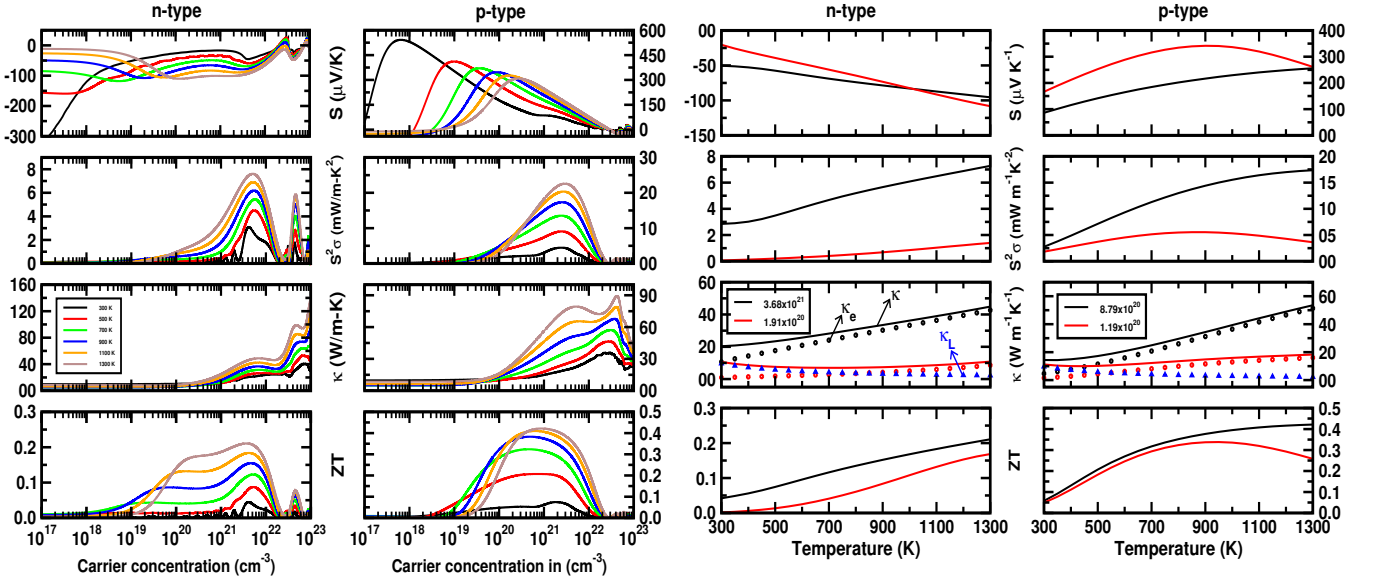


FIG. 5. Same as Fig. 3, but for ZrIrBi alloy.

ZrRhBi

Electronic Structure : ZrRhBi is the most stable among the three HHA systems with the formation energy of 725 meV/atom. It has a direct band gap of 1.021 eV, higher than the other two systems which may help in minimizing the contribution of minority carrier contributions to the Seebeck coefficient, thereby increasing the ZT value. Figure 6 shows the band structure and DOS for ZrRhBi. As seen from the band structure, both the valence and conduction band edges are almost flat near Γ point. Also the DOS near E_F shows a sharp increase making the charge carrier heavier (higher effective mass, helps in higher S value) which is a signature for it to be promising for both n-type and p-type TE applications.

Thermoelectric properties: ZrRhBi is found to have the

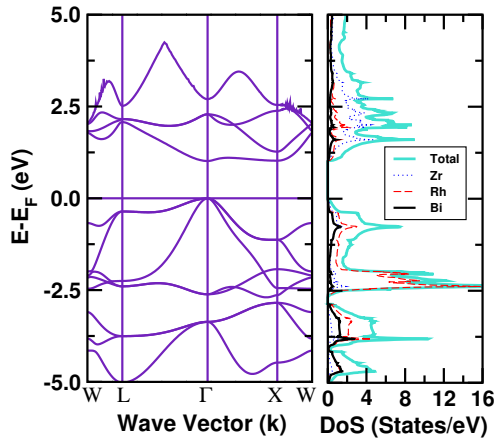


FIG. 6. Band structure(left) and atom projected DOS(right) of ZrRhBi.

highest values of TE figure of merit for both n-type and p-type systems, which is mainly attributed to the nature of bands (Figure 6). The n_c dependence of S , $S^2\sigma$, κ and ZT at various temperatures (300-1300 K) for both n-type and p-type system are shown in Figure 7. For p-type ZrRhBi, at 1300 K, the highest Seebeck coefficient ($319.89 \mu\text{VK}^{-1}$) among the three systems is obtained. The electrical conductivity ($8.7 \times 10^4 \Omega^{-1}\text{m}^{-1}$) is very low as compared to HfRhBi and ZrIrBi at optimal $(n_c)_{max}$ due to larger value of the band gap (making it difficult for electrons to excite) and thus giving a smaller power factor $\approx 8.9 \text{ mWm}^{-1}\text{K}^{-2}$, compared to the other two systems. Due to the large band gap, the electronic contribution to the thermal conductivity is also small because of the difficulty of thermally excited electron-hole pairs to reach the conduction bands. In addition, the lattice contribution to the thermal conductivity is also smaller compared to other two systems due to the highly agitated phonons. Thus in spite of having the lowest electrical conductivity, ZrRhBi has the highest ZT value (~ 0.43 at 1300 K) due to the extremely large S and lowest κ .

For n-type ZrRhBi, the Seebeck coefficients are slightly smaller than the p-type (at high T) but much higher than the S values obtained for n-type HfRhBi and ZrIrBi. Similar to p-type ZrRhBi, the electrical conductivity is quite small, but large value of S makes the power factor appreciable. ZT value in this case is equally large (0.45) as the p-type ZrRhBi.

DISCUSSION

It is well known that electronic structure plays an important role in determining the thermoelectric perfor-

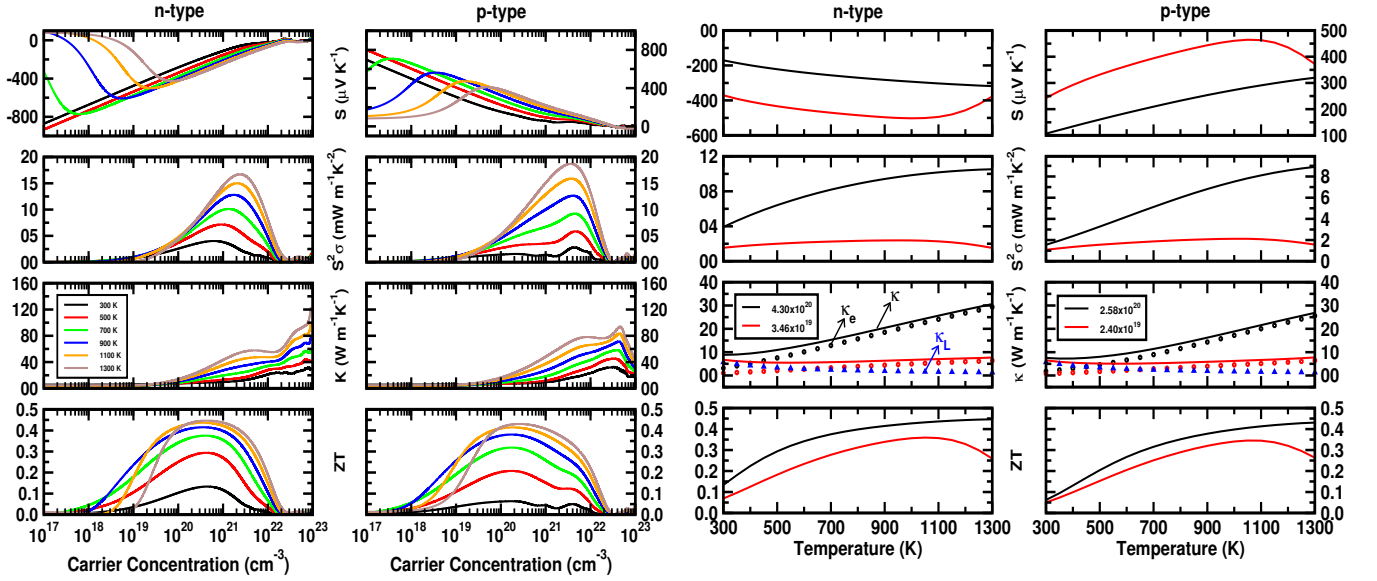


FIG. 7. Same as Fig.3, but for ZrRhBi alloy.

mance of a given material. In this section, we will explain the reason for getting high ZT values in the three candidate systems. Such plausible reasons can alone serve as a selection criteria for choosing suitable parent materials, in general, with promising TE properties.

Figure 8 shows a closer view of the band structure and atom projected density of states very near to E_F for the three systems. For HfRhBi and ZrIrBi, all the three constituent atoms have a slow rise in the number of states after E_F indicating low effective mass values which in turn reduces the n-type Seebeck coefficients. However, the p-type Seebeck coefficient for these two materials are higher due to large DOS contribution (steep rise) of the atoms before E_F (valence band edges). In contrast, for ZrRhBi, it is interesting to note that the contribution of all the three constituent atoms to the conduction as well

as valence band edge states show a steep rise in the DOS. This makes ZrRhBi to be a good TE material both as n- and p-type.

All the three systems discussed here are high temperature TE materials. At such high T, κ_L contribution becomes very small compared to κ_e (see Figure 3, 5 and 7) and hence can be neglected. This is because of the decrease in the mean free path (L_{ph}) of the thermally agitated phonons which in turn reduces κ_L ($\kappa_L \approx \frac{1}{3} v_s C L_{ph}$, where v_s and C are the velocity of sound through the material and heat capacity, respectively). Thus ZT becomes, $ZT_e = (S^2 \sigma T) / \kappa_e = S^2 / L$, using $\kappa_e = L \sigma T$. Therefore at high temperature, ZT essentially depends on the Seebeck coefficient of the material. This decrease in mean free path of phonons is most prominent in ZrRhBi because of a large difference in the masses of the constituent atoms. This is also evident from the phonon dispersion curve (see supplement [54]), which reflect strong mass scattering and hence lowest lattice thermal conductivity.

With increase in temperature, electron-hole pairs are generated giving their individual contribution to the Seebeck coefficient. The total Seebeck coefficient can be expressed as, $S = (S_n \sigma_n + S_p \sigma_p) / (\sigma_n + \sigma_p)$. Since the Seebeck coefficient for electrons and holes have opposite sign, the total S is usually lower than either of the individual contributions, unless the direct band gap is large enough to minimize the minority carrier contribution.

At moderate temperatures, the figure of merit calculated by only considering electronic thermal conductivity (ZT_e) can be misleading because in this temperature range, the κ_e values are only somewhat larger or often even comparable to κ_L values. The figure of merit can also be expressed as, $ZT = ZT_e (1 + \frac{\kappa_L}{\kappa_e})^{-1}$. From the thermal conductivity curves (Figure 3, 5 and 7) it can be

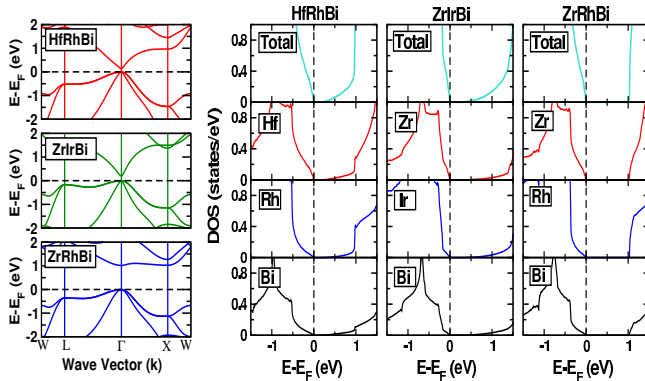


FIG. 8. Closer look of (left) band structure and (right) total and atom projected DOS for HfRhBi, ZrIrBi and ZrRhBi near E_F showing valence and conduction band edges.

Systems	T	Doping type	n_c	S	$S^2\sigma$	σ	κ_L	κ	$(ZT)_{max}$
HfRhBi	1300	n	8.32	137.88	6.79	35.71	1.98	32.31	0.27
		p	5.69	214.08	10.88	23.75		38.20	0.37
	900	n	13.16	95.33	5.16	56.83	2.86	25.23	0.18
		p	2.60	215.95	6.08	13.03		16.54	0.33
ZrIrBi	1300	n	36.77	95.55	7.28	79.68	2.22	44.88	0.21
		p	8.79	255.91	17.36	26.51		53.54	0.42
	900	n	46.99	76.15	6.11	105.34	3.20	35.50	0.15
		p	4.88	256.97	11.73	17.76		27.57	0.38
ZrRhBi	1300	n	4.30	318.23	10.53	10.39	1.31	30.64	0.45
		p	2.58	319.89	8.91	8.70		26.88	0.43
	900	n	3.63	296.66	8.79	9.98	1.88	19.05	0.42
		p	1.73	283.64	5.83	7.25		13.80	0.38

TABLE III. Highest ZT values for both n-type and p-type systems and corresponding optimal TE parameters for HfRhBi, ZrIrBi and ZrRhBi at 1300 K and 900 K. T, n_c , S, $S^2\sigma$, σ , κ_L and κ are in the units of Kelvin, 10^{20} cm^{-3} , μVK^{-1} , $\text{mWm}^{-1}\text{K}^{-2}$, $10^4 \Omega^{-1}\text{m}^{-1}$, $\text{mWm}^{-1}\text{K}^{-1}$ and $\text{mWm}^{-1}\text{K}^{-1}$ respectively.

seen that at around 300-400 K, the κ_L and κ_e values are almost equal giving, $ZT = ZT_e/2$. Thus in the low temperature range, the role of κ_L is important and should not be ignored.

Since the Seebeck coefficient decreases with increase in carrier concentration and increases with high effective mass while σ increases with small band gap and high mobility; suitable band topology, optimal carrier concentration and band gap with high mobilities are desired for promising TE applications. These factors were carefully analyzed before choosing the three systems discussed here. There are still open avenues to further enhance the thermoelectric efficiency of these materials via nanostructuring, doping with suitable elements etc. The present work, however, sets an initial path to continue on these lines.

CONCLUSION

Over the years, there has been considerable efforts on enhancing the figure of merit (ZT) of thermoelectric materials by doping, surface, nano constructions etc. This enhancement, however, very much depends on the ZT value of the parent ideal crystal. In the Half Heusler family, for example, the ZT value for the best parent materials (such as MNiSn (M=Ti, Zr, Hf), NbCoSb etc.) does not exceed beyond ~ 0.3 . One of the main motivation of the present paper is to find new parent HHs systems, with already large ZT value. Taking a hint from the band structure topology of a large combinatorial set of unreported HH compounds, we choose three systems, HfRhBi, ZrIrBi and ZrRhBi to perform a detailed electronic structure, electrical and thermal transport calculations for TE properties. All the three compounds are found to be chemically as well as mechanically strongly stable. They turn out to be efficient TE materials at high T. Table III shows the optimal TE parameters (n_c , S, σ ,

$S^2\sigma$ and κ) corresponding the highest ZT value for n- and p-type materials at two different temperatures, 1300 and 900 K. The figure of merit (ZT) for the three compounds lie in the range 0.21-0.45, with ZrRhBi having the largest value. Larger band gap ($\sim 1 \text{ eV}$) of ZrRhBi along with the occurrence of more flat bands in its band structure gives rise to higher S and hence the ZT value at high T. These compounds show an unusually high power factor ranging from 5.2 to $17.4 \text{ mWm}^{-1}\text{K}^{-2}$, responsible for high figure of merit. Although the highest possible power factor for the three systems HfRhBi, ZrIrBi and ZrRhBi are $15.49 \text{ mWm}^{-1}\text{K}^{-2}$, $22.57 \text{ mWm}^{-1}\text{K}^{-2}$ and $19.70 \text{ mWm}^{-1}\text{K}^{-2}$ respectively, however they do not correspond to the $(ZT)_{max}$ values (see Table III), showing that choosing $S^2\sigma$ as deciding factor for optimal TE performance is highly misleading, as reported in many literature. The calculated maximum power factor, optimal n- and p-type carrier concentrations corresponding to maximum ZT values for all the three systems certainly provide a guidance to the experimental work. Thermoelectric measurements on these new compounds are strongly recommended.

ACKNOWLEDGEMENT

AA acknowledges DST-SERB (SB/FTP/PS-153/2013) for funding to support this research. Enamullah (an institute post-doctoral fellow) acknowledges IIT Bombay for financial support.

* aftab@phy.iitb.ac.in

- [1] Romain Gautier, Xiuwen Zhang, *et al.*, Nature Chemistry **7**,308-316 (2015).
- [2] T. M. Tritt, Science **272**, 1276-1277 (1996); Science **283**, 804-805 (1999).

- [3] F. J. DiSalvo, *et al.*, Science **285**, 703 (1999).
- [4] D. Y. Chung, T. H. Hogan, P. Brazis, M. Rocci-Lane, C. Kannewurf, M. Bastae, C. Uher, and M. G. Kanatzidis, Science **287**, 1024-1026 (2000).
- [5] R. T. Littleton IV, Terry M. Tritt, J. W. Kolis, and D. R. Ketchum, Phys. Rev. B **60**, 13453 (1999).
- [6] G. S. Nolas, M. Kaeser and T. M. Tritt, Appl. Phys. Lett. **77**, 1855 (2000).
- [7] B. C. Sales, D. Mandrus and R. K. Williams, Science **272**, 1325 (1996).
- [8] A. L. Pope, Terry M. Tritt, M. A. Chernikov and M. Feuerbacher, Appl. Phys. Lett. **75**, 1854 (1999).
- [9] Tanja Graf, Claudia Felser and Stuart S.P. Parkin, Progress in Solid State Chemistry **39** (2011) 1-50.
- [10] G. S. Nolas, J. Poon and M. Kanatzidis, MRS Bulletin, Volume **31**, March 2006.
- [11] Shuo Chen and Zhifeng Ren, Materials today, Volume **16**, Number 10, (2013).
- [12] Wei-Shu Liu, Qinyong Zhang, Yucheng Lan, *et al.*, Adv. Energy Mater. 2011, **1**, 577-587.
- [13] B. Poudel, *et al.*, Science **320** (2008) 634.
- [14] Aaron D. LaLonde, Yanzhong Pei and G. Jeffrey Snyder, Energy Environ. Sci., 2011, **4**, 2090.
- [15] Qian Zhang, Feng Cao, Weishu Liu, *et al.*, J. Am. Chem. Soc. 2012, **134**, 10031-10038.
- [16] Xun Shi, Jiong Yang, James R. Salvador, *et al.*, J. Am. Chem. Soc. 2011, **133**, 7837-7846.
- [17] Qing Jie, Hengzhi Wang, Weishu Liu, *et al.*, Phys. Chem. Chem. Phys., 2013, **15**, 6809.
- [18] Shuo Chen, Kevin C. Lukas, Weishu Liu, *et al.*, Adv. Energy Mater. 2013, **3**, 1210-1214.
- [19] Xiao Yan, Weishu Liu, Shuo Chen, *et al.*, Adv. Energy Mater. 2013, **3**, 1195-1200.
- [20] Mona Zebajadi, Giri Joshi, Gaohua Zhu, *et al.*, Nano Lett. 2011, **11**, 2225-2230.
- [21] Bo Yu, Mona Zebajadi, Hui Wang, *et al.*, Nano Lett. 2012, **12**, 2077-2082.
- [22] Q. Shen, L. Chen, T. Goto, *et al.*, Applied Physics Letters **79**, 4165 (2001).
- [23] S. Sakurada and N. Shutoh, Applied Physics Letters **86**, 082105 (2005).
- [24] Cui Yu, Tie-Jun Zhu, Rui-Zhi Shi, *et al.*, Acta Materialia **57** (2009) 2757-2764.
- [25] Yoshisato Kimura, Yukio Tamura and Takuji Kita, Applied Physics Letters **92**, 012105 (2008).
- [26] Y Xia, V Ponnambalam, S Bhattacharya, *et al.*, J. Phys.: Condens. Matter **13** (2001) 77-89.
- [27] Ting Wu, Wan Jiang, Xiaoya Li, *et al.*, Journal of Applied Physics **102**, 103705 (2007).
- [28] Shanming Li, Huaizhou Zhao, Dandan Li, *et al.*, Journal of Applied Physics **117**, 205101 (2015).
- [29] ICSD, <https://icsd.fiz-karlsruhe.de/search/basic.xhtml>
- [30] P. Villars and L. D. Calvert, Pearson's handbook of crystallographic data for intermetallic phases, 2nd Edition, ASM International, Materials Park, Ohio, USA, 1991.
- [31] Vikram, Jiban Kangsabanik, Enamullah and Aftab Alam (Unpublished).
- [32] Janusz Tobol and Jacques Pierre, Journal of Alloys and Compounds **296** (2000) 243-252.
- [33] Hem Chandra Kandpal, Claudia Felser and Ram Sesshadri, J. Phys. D: Appl. Phys. **39** (2006) 776-785.
- [34] B R K Nanda and I Dasgupta, J. Phys.: Condens. Matter **15** (2003) 7307-7323.
- [35] Jiong Yang, Huanming Li, Ting Wu, *et al.*, Adv. Funct. Mater. 2008, **18**, 2880-2888.
- [36] D. F. Zou, S. H. Xie, Y. Y. Liu, *et al.*, Journal of Applied Physics **113**, 193705 (2013).
- [37] G. Rogl, A. Grytsiv, M. Grth, *et al.*, Acta Materialia **107** (2016) 178-195.
- [38] Takeyuki Sekimoto, Ken Kurosaki, Hiroaki Muta, *et al.*, Journal of Applied Physics **99**, 103701 (2006).
- [39] Takeyuki Sekimoto, Ken Kurosaki, Hiroaki Muta, *et al.*, Materials Transactions, Vol. **48**, No. 8 (2007) pp. 2079 to 2082.
- [40] Yoshiyuki Kawaharada, Ken Kurosaki, Hiroaki Muta, *et al.*, Journal of Alloys and Compounds **381** (2004) 9-11.
- [41] P. Hohenberg and W. Kohn, Phys. Rev. **136**, B865 (1964).
- [42] G. Kresse and J. Furthmüller, Comput. Mater. Sci. **6**, 15 (1996).
- [43] G. Kresse and J. Furthmüller, Phys. Rev. B **54**, 011169 (1996).
- [44] G. Kresse and J. Hafner, Phys. Rev. B **47**, 558 (1993).
- [45] P. E. Blochl, Phys. Rev. B **50**, 17953 (1994).
- [46] J. P. Perdew, K. Burke, and M. Ernzerhof, Phys. Rev. Lett. **77**, 3865 (1996).
- [47] Peter E. Blöchl, O. Jepsen and O. K. Andersen, Phys. Rev. B **49**, 16223 (1994).
- [48] Giovanni Pizzi, Dmitri Volja, Boris Kozinsky, Marco Fornari, Nicola Marzari, Computer Physics Communications, Volume **185**, Issue 1, January 2014, Pages 422-429.
- [49] AA Mostofi, JR Yates, G Pizzi, YS Lee, I Souza, D Vanderbilt, N Marzari, Comput. Phys. Commun. **185**, 2309 (2014).
- [50] N. Marzari and D. Vanderbilt, Phys. Rev. B **56**, 12847 (1997).
- [51] I. Souza, N. Marzari and D. Vanderbilt, Phys. Rev. B **65**, 035109 (2002).
- [52] W. Li, J. Carrete, N. A. Katcho, and N. Mingo, Comp. Phys. Commun. **185**, 1747-1758 (2014).
- [53] Atsushi Togo and Isao Tanaka, Scr. Mater., **108**, 15 (2015).
- [54] See Supplementary material at [URL] for more details (2016).